Structural Investigations of LiFePO$_4$ Electrodes by Fe X-ray Absorption Spectroscopy

Aniruddha Deb*

Environmental Energy Technologies Division, Ernest Orlando Lawrence Berkeley National Laboratory, Berkeley, California 94720

Uwe Bergmann

Stanford Synchrotron Radiation Laboratory, Sand Hill Road, Menlo Park, California 94025

Elton J. Cairns

Environmental Energy Technologies Division, Ernest Orlando Lawrence Berkeley National Laboratory, Berkeley, California 94720, and Department of Chemical Engineering, University of California, Berkeley, California 94720

Stephen P. Cramer

Structural Biology Division, Ernest Orlando Lawrence Berkeley National Laboratory, Berkeley, California 94720, and Department of Applied Science, University of California, Davis, California 95616

Fe K-edge X-ray absorption near-edge spectroscopy (XANES) and extended X-ray absorption fine structure (EXAFS) have been performed on LiFePO$_4$, and on electrodes containing this material to determine the local atomic and electronic structure and their stability with electrochemical cycling (repeated charging and discharging). Comparison of the XANES data for the powder sample, uncycled electrode, and cycled electrodes 7SG and 9SG reveals that the Fe ions are octahedrally coordinated and in the Fe^{2+} state. Even after repeated charging and discharging, the structure of the LiFePO$_4$ cycled electrodes (7SG, cycled 64 times, and 9SG, cycled 21 times) did not change and hence the material possesses very desirable characteristics for an electrode. This makes it an excellent choice for long cycle life Li-ion battery applications.
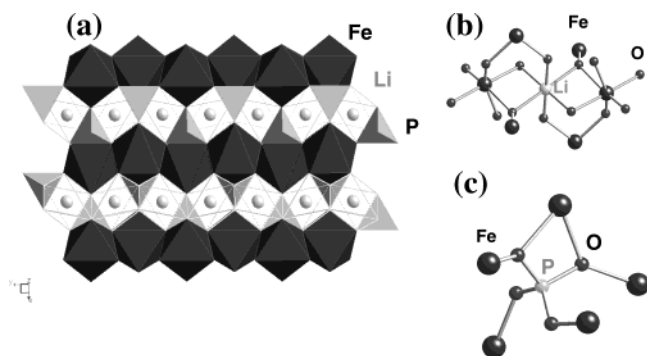
Introduction

The emergence of portable telecommunications, computer equipment and, ultimately, electric and hybrid vehicles has created a growing demand for improvements in energy storage devices that are cost-effective, operate for a longer time, and are smaller in size and weight.[1] Transition metal oxides have been investigated as active cathode materials because of their high potential versus Li/Li$^+$, and in many of the materials a large proportion of the lithium can be inserted/extracted reversibly.

In several Fe-containing compounds such as Li$_3$FeN$_2$,[2] LiFe$_5$O$_8$,[3] Fe$_3$O$_4$,[4] Fe$_2$O$_3$,[5] and FePS$_3$,[6] lithium insertion has been investigated earlier. These compounds rely on an Fe^{3+}/Fe^{2+} redox couple and hence have a low open-circuit voltage versus Li/Li$^+$. The substitution of oxygen by a polyanion (MO$_4$$^{3-}$) such as sulfate or phosphate lowers the Fermi level of the Fe^{3+}/Fe^{2+} redox couple and thereby increases the cell potential.[7−9] This effect is more pronounced for compounds with less covalent Fe−O bonds, where M in MO$_4$$^{3-}$ determines the strength of the Fe−O covalency via an inductive effect.[10] Since the demonstration of reversible electrochemical lithium insertion−extraction for LiFePO$_4$ in 1997,[10] lithium transition metal phosphates with an ordered olivine structure, LiMPO$_4$ (M = Co, Ni, Mn, Fe, Cu) have attracted much attention as promising new cathode materials for rechargeable lithium batteries.[12−15] One of the most promising candidates for rechargeable lithium batteries is LiFePO$_4$, with a theoretical capacity of 170 mAh/g[11] and a voltage of >3.4 V versus Li/Li$^+$. LiFePO$_4$ is inexpensive, nontoxic, nonhygroscopic, and environmentally friendly. It occurs in nature as the mineral triphylite, which has an orthorhombic unit cell (space group *Pmna*)[16] as shown in Figure 1, and often contains varying amounts of manganese as in LiFe$_x$Mn$_{1-x}$PO$_4$. Both Li and M atoms are in octahedral sites with Li located in the 4a and M in the 4c positions. The oxygen atoms are nearly hexagonal closed-packed and the M atoms occupy zigzag chains of corner-shared octahedra running parallel to the *c*-axis in alternate a−c planes. These chains are bridged by corner- and edge-sharing (PO$_4$$^{3-}$) polyanions to form a host structure with strong three-dimensional bonding. The Li$^+$ ions in the 4a sites form continuous linear chains of edge-shared octahedra running parallel to the *c*-axis in the other *a−c* planes. The P$_{tet}$−O−Fe$_{oct}$ linkage in the structure induces a super-exchange interaction that tunes the Fe^{3+}/Fe^{2+} redox energy to useful levels (3.4 V).[11] The stable nature of the olivine-type structure having a (PO$_4$$^{3-}$) polyanion with a strong P−O covalent bond provides not only excellent cycle-life but also a safe system. When the electrode is fully charged, the reactivity with regard to the combustion reaction with the organic electrolyte is low.[15]

* Author to whom correspondence should be addressed at Lawrence Berkeley National Laboratory, One Cyclotron Road, MS 70-108B, Berkeley, CA 94720. Phone: (510) 486-7055. Fax: (510) 486-7303. E-mail: ADeb@lbl.gov.

Structural Investigations of LiFePO$_4$ Electrodes

J. Phys. Chem. B, Vol. 108, No. 22, 2004 **7047**

Figure 1. (a) The structure of LiFePO$_4$. The P atoms occupy tetrahedral 4c sites (light shading) and the Fe atoms occupy octahedral 4c sites (dark shading). The light shaded circles represent the Li ions. The oxygen atoms are arranged in a hexagonal closed-packed arrangement. (b) A view of the close neighbors of the Li ion where the small dark circles represent the oxygen atoms and the big dark circles represent the Fe atoms. (c) A view of the close neighbors of the P atom where the small dark circles represent the oxygen atom and the big dark circles represent the Fe atoms.

Synchrotron-based X-ray absorption spectroscopy is a very useful tool to investigate the structural and electronic properties of this compound. X-ray absorption near-edge spectroscopy (XANES) is an element-specific technique sensitive to the local atomic and electronic structure of the element of interest.[17] XANES and extended X-ray absorption fine-structure spectroscopy (EXAFS) studies have revealed details about the local coordination, site symmetry, oxidation state, and bond character in Mn oxides and Mn-containing molecular compounds.[18−21] But until now, to the best of our knowledge, there have been no reports in the literature of XANES and EXAFS studies on LiFePO$_4$ and LiFe$_x$Mn$_{1−x}$PO$_4$. To study the atomic and electronic structure of these materials and understand the changes occurring upon cycling, we performed Fe XANES and EXAFS on these materials and electrodes extracted from cycled cells.

Experimental Procedures

The LiFePO$_4$ powder used in this study was synthesized using the starting materials Fe(NO$_3$)$_3$·9H$_2$O (iron nitrate, Aldrich), Li-(CH$_3$COO)$_2$·2H$_2$O (lithium acetate, Aldrich), H$_3$PO$_4$ (phosphoric acid, Sigma), and HOCH$_2$COOH (glycolic acid, Aldrich). The metal compounds were first dissolved in phosphoric acid and deionized water. This solution was mixed until homogeneous and was added to glycolic acid (1:2 metal/glycolic acid ratio). Ammonium hydroxide was added to the solution to adjust the pH between 8.5 and 9.5. The solution was heated to 70−80 °C under N$_2$ until a gel was formed. This gel was then transferred to an alumina boat, heated slowly to 500 °C under flowing N$_2$, and then decomposed at that temperature for 10 hours. The resultant powders were ground, dried, and then heated to 600 or 700 °C under a flow of N$_2$ gas, for 5−15 h. The reader is referred to Doeff et al.[22] for further details for the description of the preparation of the electrodes containing LiFePO$_4$. The product was a single phase, as was verified by X-ray diffraction (XRD). In addition to the powder, three electrodes were also studied, one uncycled and two cycled electrodes extracted from coin cells and designated as 7SG and 9SG, respectively. A quantity of 2032 coin cells containing LiFePO$_4$ electrodes 7SG and 9SG, 1 M LiPF$_6$ in ethylene carbonate/dimethyl carbonate (EC/DMC), and lithium anodes were cycled galvanostatically using a Macpile potentiostat/galvanostat (Bio Logic, Claix, France). The 7SG electrode was cycled 64 times at a current density of 0.027 mA/cm^2 (or 3.5 mA/g) and 0.055 mA/cm^2 (or
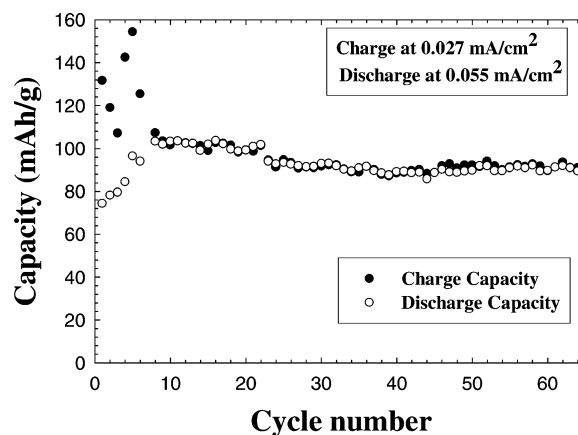
Figure 2. Capacity versus cycle number for the 7SG cycled electrode shown for the full 64 cycles. The charge and discharge current densities are 0.027 mA/cm^2 and 0.055 mA/cm^2, respectively.[22]
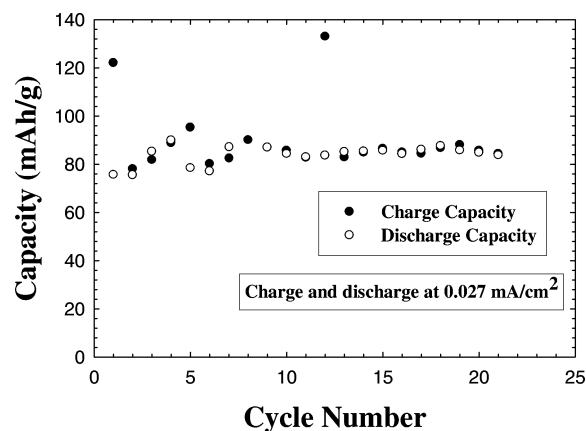
Figure 3. Capacity versus cycle number for the 9SG cycled electrode shown for the full 21 cycles. The constant charging and discharging current density is 0.027 mA/cm^2.[22]

7.2 mA/g) for charge and discharge between the limits of 3.9 and 2.5 V, respectively. One electrode was extracted from a cycled cell (7SG) at the end of the 64th discharge. The discharge capacities as a function of cycle numbers are shown in Figure 2. There is a small loss of capacity on cycling, and the last discharge corresponds to about 90 mAh/g. The 9SG electrode was cycled 21 times at a constant current density of 0.027 mA/cm^2 (or 3.5 mA/g) between the limits of 3.9 and 2.5 V. The electrode was extracted from the cycled cell at the end of the 21st discharge. The discharge capacities as a function of cycle numbers are shown in Figure 3.

Preparation of the 7SG and 9SG electrode samples was carried out in an Ar-filled glovebag. The composite electrodes, containing the powder cathode, Kynar PVdF binder, SFG-6, and compressed acetylene black (laminated electrodes contain 80 wt % active material, 8 wt % Kynar PVdF binder, 6 wt % SFG-6 synthetic flake graphite, and 6 wt % compressed acetylene black) were diced and mixed in a 1:10 w/w ratio with anhydrous boron nitride (BN) using a mortar and pestle after removal. All the other samples in this study were prepared at a similar dilution. Once the powder or the electrode samples were well mixed with BN, approximately 0.180 g of the mix was pressed in the form of a pellet and placed in a 0.19 cm thick sample holder (1.32 cm in diameter), and then enclosed with 0.005 cm Kapton tape.

The X-ray absorption measurements, which included both XANES and EXAFS techniques, were performed on the wiggler beam line 9-3 of the Stanford Synchrotron Radiation Laboratory

TABLE 1: Positions for the XANES Spectral Features as Shown in Figures 4 and 5. (Positions of the features represented by the Greek letters were obtained from the second derivatives (Figure 5), whereas the other peak positions shown here were obtained using the EXAFSPAK. The energy positions mentioned here are in units of eV.)

sample	α	β	γ	ϵ	η	A	B	C
powder	7111.82	7122.03	7125.12	7126.84	7131.43	7126.44	7138.32	7172.21
uncycled electrode	7111.82	7122.03	7125.12	7126.84	7131.43	7126.44	7138.32	7172.21
7SG, cycled	7111.95	7122.16	7125.25	7126.97	7131.56	7126.57	7138.45	7172.34
9SG, cycled	7111.95	7122.16	7125.25	7126.97	7131.56	7126.57	7138.45	7172.34

(SSRL), with the storage ring operating at 3.0 GeV with 100 mA current at the top of the fill. A Si(220) double crystal monochromator was used for energy selection. To avoid the higher harmonics, the incident beam was detuned to 35% of maximum intensity. The intensities of the incident and the transmitted X-rays were monitored by nitrogen-filled ionization chambers. The monochromator was scanned in energy from 312 eV below to 1050 eV above the Fe K absorption edge (7112 eV). The Fe K-edge X-ray absorption spectra were measured in transmission mode at room temperature. Transmission ion chambers were used to measure the incident (I_0), transmitted (I_t), and reference (I_{ref}) signals. A 9 μm thick Fe foil was used as a reference, and both foil and I_{ref} detectors were positioned behind the sample along the direction [X-ray beam/I_0-detector/Sample/I_{Sample}-detector/Fe-foil/I_{ref}-detector]. Data were collected using a 0.1 eV step size through the edge region and a variable step size, giving $\Delta k_{max} = 0.05$ Å^{-1} for the EXAFS region. Reduction of the absorption data was performed using the EXAFSPAK analysis package available from SSRL. Transmission data from scans of each sample were averaged, and the background was subtracted using a straight line from 6800 to 7085 eV. The XANES were normalized using a quartic spline fit through the background. Second derivatives were obtained after smoothing with a third-order polynomial over a 1.5 eV window. The $\chi(k)$ function was weighted with k^3 to account for damping of oscillations with increasing k. The radial structure function was obtained by Fourier transform of $k^3\chi(k)$ using a k-range of 1.5−16.4 Å^{-1}. The k range was adjusted until in the radial structure function no unexpected peaks were seen below the anticipated Fe−O distance. The EXAFSPAK was also used to fit the EXAFS spectrum with theoretical scattering paths, which were generated with FEFF 8 code.[23]

Results and Discussion

The XANES of all four LiFePO$_4$-based samples are shown in Figure 4. To facilitate comparison, the preedge region of each of the respective spectra here has been magnified by a factor of 10 for clarity in Figure 4. The energy positions of the salient features of the XANES spectra are shown in Table 1. The positions A, B, and C as defined were identified using the EXAFSPAK. Positions of the other spectral features which are also shown in Table 1 utilizing the Greek letters were identified from the XANES second derivatives shown in Figure 5. For a better understanding and clarity we here have shown only a smaller energy range for the XANES second derivative as compared to the XANES which has been shown in Figure 4. The features which have been identified as α, ϵ, and η were obtained from the local minima whereas the features which have been depicted as β and γ are the small shoulder-like structures that have been identified in the second derivative. Here the preedge peak in Figure 4 is the most useful feature to discriminate between the oxidation state and coordination number of Fe. This peak represents an s−d like transition and is thus dipole forbidden, but it becomes partially allowed by mixing of the d-states of the transition metal with the p-states of the surrounding oxygen atoms. Its energy position depends
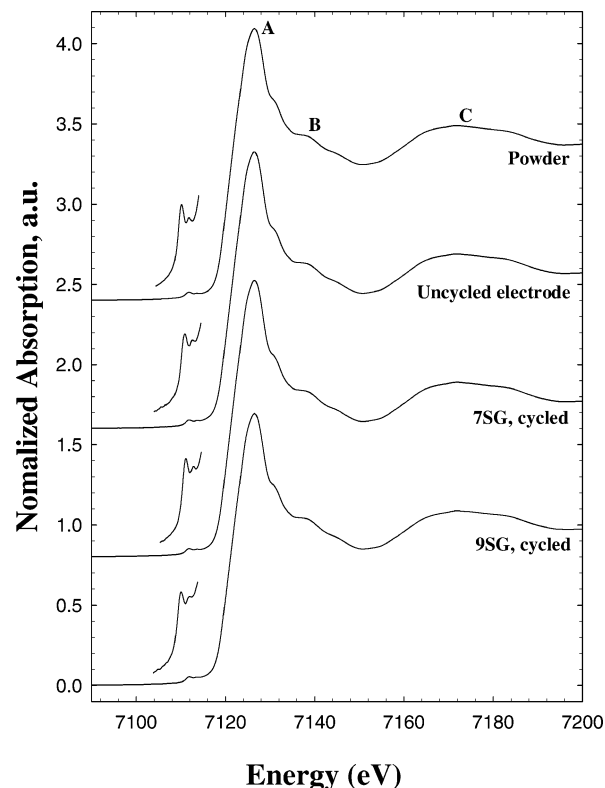
Figure 4. The normalized Fe K-edge XANES of powder, uncycled electrode, 7SG cycled electrode, and 9SG cycled electrode. The preedge of each of the respective spectra in the inset are magnified by a factor of 10.

mainly on the Fe oxidation state, whereas its intensity depends on the geometry around Fe,[24,25] so that it will be virtually zero in case of regular octahedral symmetry (O_h) around the absorber, and it will reach its maximum in case of tetrahedral coordination (T_d). A first observation of Figure 4 reveals that in the LiFePO$_4$ powder XANES the Fe are octahedrally coordinated by oxygen. This can be concluded from the observation of the shape of the preedge region. The preedge region is assigned to 1s→3d transitions, and a weak intensity in this region indicates an octahedral coordination as opposed to the tetrahedral coordination from which a strong preedge intensity is found.[18,20] This can be best understood if we consider the XANES spectra of FePO$_4$,[26] as comparison, where FePO$_4$ is usually considered as a perfect model compound for Fe in tetrahedral coordination.[27] As reported earlier by Berlier et al.,[26] they observed in FePO$_4$ a presence of a strong preedge intensity. But unlike FePO$_4$, the α-Fe$_2$O$_3$ and Fe(acac)$_3$ (acac = acetylacetonate) where Fe has been in the octahedral symmetry shows a weak preedge intensity similar to that which we observe here in LiFePO$_4$. Another interesting feature of the XANES spectra shown in Figure 4 is the 1s−3d preedge peak observed for the powdered LiFePO$_4$ sample for Fe^{2+} is at 7111.8 eV which is at lower energies than that for Fe^{3+} in FePO$_4$ where the preedge peak is at 7114.2 eV as observed by Berlier et al.[26] If we compare the energy positions of the spectral features shown in Table 1 between

Structural Investigations of LiFePO₄ Electrodes

J. Phys. Chem. B, Vol. 108, No. 22, 2004 **7049**
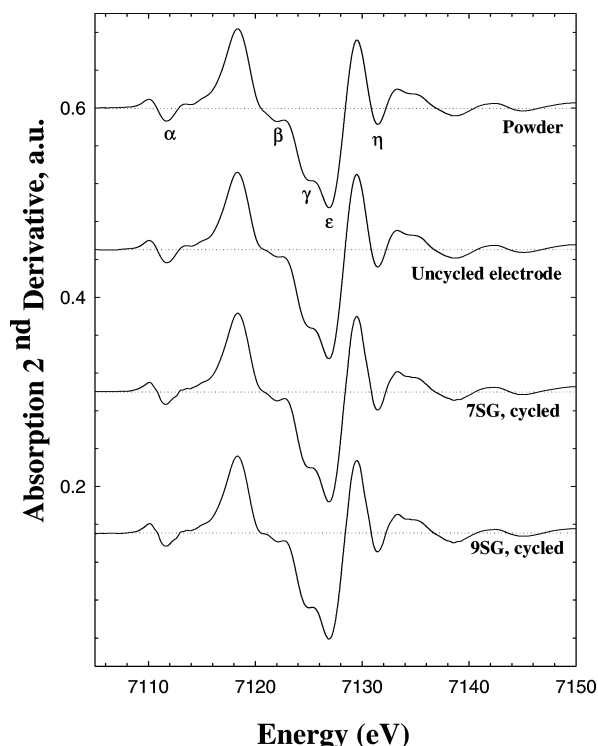
Figure 5. Comparison of Fe K-edge XANES second derivative from the powder, uncycled electrode, 7SG cycled electrode, and 9SG cycled electrode.

Figure 6. Normalized background-subtracted k^3-weighted [$k^3\chi(k)$] Fe EXAFS spectrum for powder, uncycled electrode, 7SG cycled electrode, and 9SG cycled electrode, respectively.

powder LiFePO₄ and FePO₄, the slightly lower main peak (A) energy in LiFePO₄ is due to the lower valence state of Fe in LiFePO₄. For the Fe in FePO₄ with a higher valence state, the electrons are more strongly bound to the Fe nucleus; hence, the absorption edge features are shifted to a higher energy.

Next, the effects of cycling LiFePO₄ are discussed. To begin with, the shape of the edge and the preedge of the cycled electrodes 7SG and 9SG are similar to those we have observed for the powdered and the uncycled electrode, indicating that the octahedral coordination is not changed as a result of the cycling process, unlike the results observed in LiMn₂O₄.[28] The XANES observed has been consistent with the behavior of other transition-metal compounds with octahedral coordination,[29,30] where the XANES possess an edge with a single, smooth maximum as the three 4p states are degenerate and give rise to the molecular orbital t₁ᵤ. The position of the 1s−3d preedge peak observed for the cycled electrodes is almost same as that for powdered LiFePO₄ (7111.9 eV, which is consistent with the observation of the preedge peak at 7112.5 eV of a similar Fe²⁺ model compound FeCp₂ (Cp = cyclopentadienyl) studied earlier by Berlier et al.[26]), indicating the Fe²⁺ state in the discharged cycled electrodes. The data of Figure 4 and Figure 5 show that the powder and cycled electrodes possess similar characteristics (considering also the positions of α, β, γ, ε, and η as shown in Table 1), suggesting that the local structure is not significantly altered by repeated cycling (charging and discharging) of the electrodes 7SG and 9SG. This is also particularly evidenced by the preedge regions. It is also seen from Table 1, the XANES and the second derivate features α, β, γ, ε, η, A, B, and C are all shifted by 0.13 eV for the cycled elctrodes as compared with the powder and the uncycled LiFePO₄ electrode. As seen from the earlier study of Davenport et al.,[31,32] for the cathodic reduction of iron oxide passive film, there is a progressive evolution of the XANES spectra with a shift of approximately 4 eV, while moving from Fe₂O₃ toward
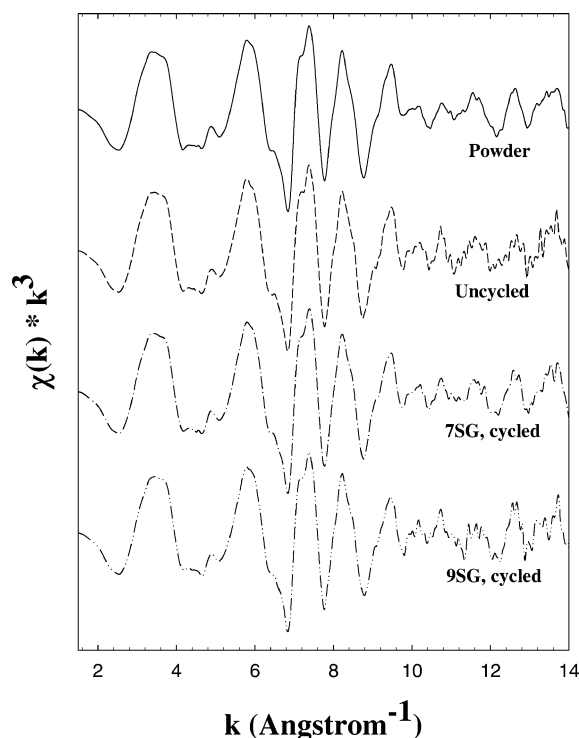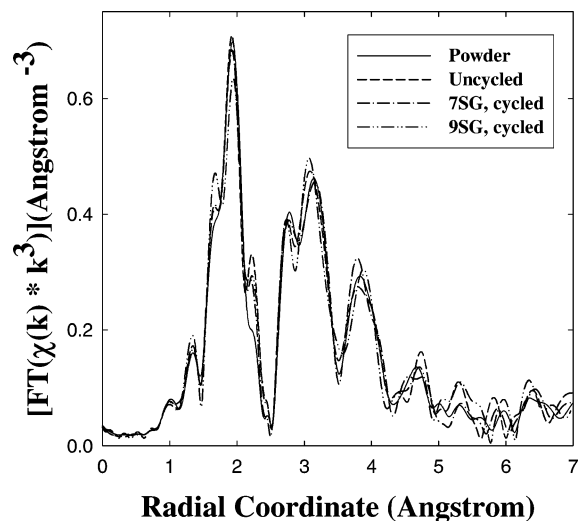
Figure 7. Radial structure function from the Fourier transform of the k^3-weighted Fe K-edge EXAFS. (*k*-range = 1.5−16.4 Å).

Fe₃O₄ and to Fe²⁺ (aq). Hence taking this 4 eV XANES shift from Fe³ to Fe²⁺, here in this study (from Table 1) there is a maximum of 3.3% Fe³⁺ contribution in the cycled electrodes.

In the EXAFS analyses, the FEFF program[23,33] was employed for the theoretical calculation of the scattering paths, and the EXAFSPAK program was employed for nonlinear least-squares fitting the Fourier transform (FT) of the EXAFS data. The coordination number, radial distances, and Debye−Waller factor were, in general, all allowed to vary for each path, while one E_0 value was used for every scattering path. The normalized, background-subtracted and k^3-weighted Fe K-edge EXAFS spectrum ($k^3\chi(k)$-function) of the powdered, uncycled, 7SG and 9SG cycled electrodes, measured at room temperature are shown in Figure 6. Only subtle changes are observed to take place between the powdered, uncycled electrode and the 7SG, 9SG

a

b
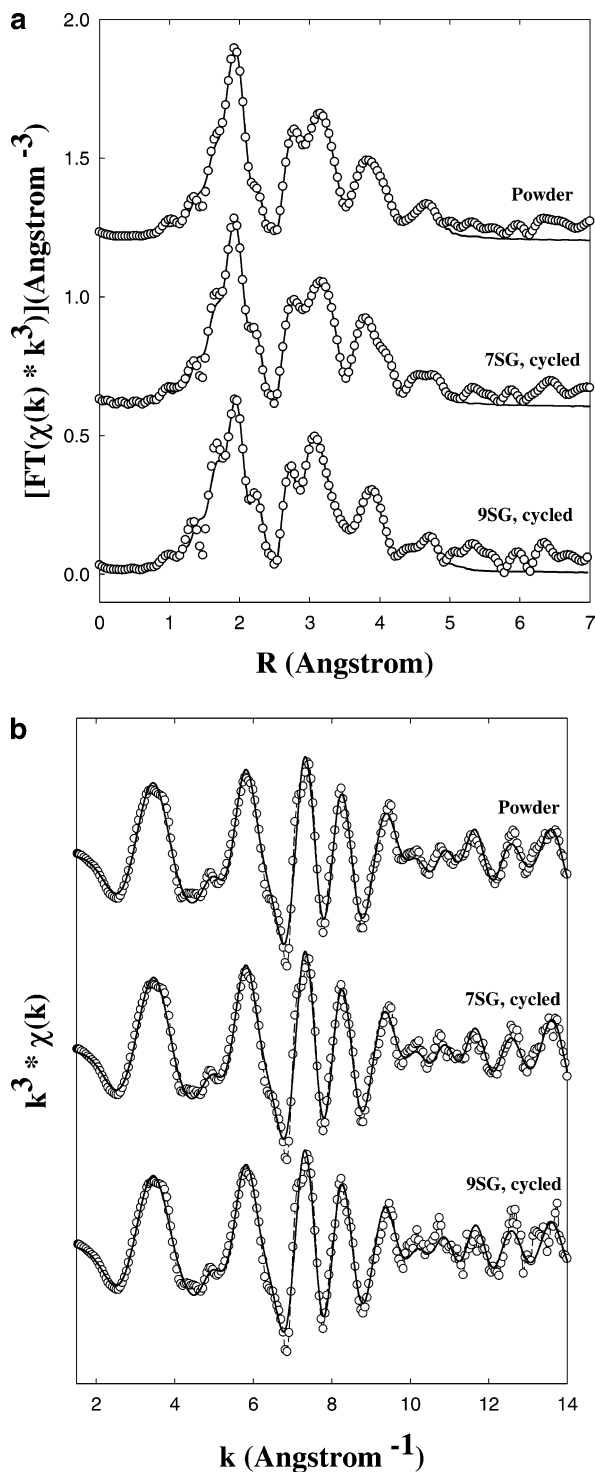
Figure 8. (a) Fit to the Fourier transform of the k^3-weighted Fe K-edge EXAFS spectrum (R-range = 1.2−4.9 Å). The symbols represent the experimental data and the thick solid lines represent the fit. The fitted parameter values are shown in Table 2. (b) Results of the curve-fitting analysis of $k^3\chi(k)$ EXAFS for the powder sample, 7SG and 9SG cycled electrodes. The open symbols and broken lines represent the experimental raw data and the thick solid line represents the fit of the sum of the paths.

cycled electrodes. The radial structure function obtained by Fourier transform of $k^3\chi(k)$ over the k-space range between 1.5 and 16.4 Å^{-1} are shown in Figure 7.

We observe that in the radial structure function two strong peaks are seen at the start (at about 1.9 and 2.8 Å) and two weaker ones are observed at higher distances (at about 3.8 and

TABLE 2: Structural Parameters for the Powder Sample, 7SG and 9SG Cycled Electrodes Derived from Fitting the Fe-edge EXAFS Spectra. (Numbers in parentheses are statistical errors of the last significant digit.)[a]

sphere	Z_a−Z_b	CN	R(Å)	σ^2(Å^2 10^{-3})
		Powder Sample		
		F-factor = 0.544×10^2		
1st	Fe−O	2	1.989(2)	2.1(5)
1st	Fe−O	2	2.150(4)	4.5(8)
1st	Fe−O	2	2.252(3)	5.6(6)
2nd	Fe−P	1	2.847(5)	1.9(1)
2nd	Fe−P	2	3.138(7)	4.1(2)
2nd	Fe−P	2	3.274(8)	8.4(3)
3rd	Fe−Fe	4	3.852(5)	5.5(1)
4th	Fe−Fe	2	4.626(7)	8.5(3)
		7SG Cycled Electrode		
1st	Fe−O	2	1.981(3)	2.0(4)
1st	Fe−O	2	2.152(5)	4.0(7)
1st	Fe−O	2	2.247(4)	5.4(5)
2nd	Fe−P	1	2.842(6)	2.0(2)
2nd	Fe−P	2	3.148(8)	4.3(3)
2nd	Fe−P	2	3.277(8)	7.7(4)
3rd	Fe−Fe	4	3.851(4)	5.3(2)
4th	Fe−Fe	2	4.626(6)	9.1(2)
		9SG Cycled Electrode		
1st	Fe−O	2	1.974(2)	1.8(5)
1st	Fe−O	2	2.149(5)	4.4(8)
1st	Fe−O	2	2.249(3)	5.0(6)
2nd	Fe−P	1	2.843(6)	2.2(2)
2nd	Fe−P	2	3.143(7)	5.1(4)
2nd	Fe−P	2	3.270(8)	6.9(5)
3rd	Fe−Fe	4	3.851(3)	5.7(3)
4th	Fe−Fe	2	4.620(5)	8.9(4)

[a] Z_a−Z_b = central absorber and scattering atom (or path) correlation, CN = coordination number, R = interatomic distance, σ^2 = Debye−Waller disorder parameter. The F−factor represents the sum of the squares of the differences between experimental and calculated values. (F= $[\sum k^6(\chi_{expt} - \chi_{calcd})^2/\sum k^6\chi_{expt}^2]^{1/2}$).

4.6 Å). The peak positions in the radial structure function are close to the radius of the backscattering shells. But in order to obtain the correct information on the radius of the shells, amplitude and phase corrections are necessary. This can be achieved by either using a reference sample which has a similar atomic structure or by simulating the interference pattern of the XAS spectrum, utilizing the theoretically calculated scattering contributions. Since here we know the structure of LiFePO$_4$ from XRD, we utilized the latter possibility to analyze the spectra by using different sets of scattering paths obtained by the ab initio FEFF8 calculation.

Quantitative analyses were performed on the first four peaks appearing in the radial structure function between $R = 0.5$ and 4.5 Å (see Figure 7). We used *Pmna* space group symmetry to generate the scattering paths with the FEFF 8 code. The input file for FEFF 8 was generated utilizing the ATOMS program (Ver. 3, beta 7),[34] where the coordinates of the atoms in the unit cells were taken from the literature as well as from our XRD data using the PowderCell (Ver. 2.4).[35] Our fitting procedure is similar to that described in Thompson et al.[36] There are some differences in our method in determining S_0^2 and ΔE_0. In the first cycle of our fitting, the coordination number N and distance R of the first shell (Fe−O) were fixed at the XRD values to establish good starting values for S_0^2, σ^2, ΔE_0 (the difference between the threshold Fermi level of an electron gas used by FEFF and the actual threshold energy associated with the atom cluster being studied). In the second round of fitting, N, R, σ^2, and ΔE_0 were allowed to vary freely. The value of ΔE_0 determined in this round was used for all the shells of LiFePO$_4$. The second and higher shells were then added in

Structural Investigations of LiFePO₄ Electrodes

J. Phys. Chem. B, Vol. 108, No. 22, 2004 **7051**

sequence. The values of N, R, and σ^2 for each of these shells were allowed to vary freely. Paths that contribute significantly were included in the final round of fitting, while other paths were not included. The criteria used for "significant contribution" were that including the shell in the fit (1) improved the fit to the EXAFS and radial structure function visually and (2) improved the goodness of fit parameter (*F*-value, which is the sum of the squares of the differences between experimental and calculated curves) as in EXAFSPAK. From the fit of powder LiFePO₄ (as shown in Figure 8a) the first peak around 1.9 Å in the FT corresponds to the Fe−O interaction in the first coordination sphere, the second one around 3.1 Å is the Fe−P interaction in the second coordination sphere. At further distances, the peak at around 3.8 Å represents the Fe−Fe interaction in the third coordination sphere, and the peak around 4.7 Å represents the second Fe neighbor at the central Fe atom which are in good agreement with also the XRD values. The fit to the first peak for the powder sample, confirmed an octahedral 6-fold Fe−O bond in the first coordination shell. The final results from the fit analysis of the radial structure function over the first four peaks for the powder, 7SG and 9SG cycled electrodes are given in Table 2. The fit results with the $k^3\chi(k)$ spectra in the *k*-space are shown in Figure 8b. Finally, as is seen from the results of the fit in Figure 8a (also in Table 2), the fitted distance of the scattering paths for the Fe−O, Fe−P, and the Fe−Fe varied by less than 0.01 Å. These findings indicate strongly that the local atomic structure after repeated cycling remains unchanged, reinforcing the suitability of this material for Li-ion battery applications.

Conclusions

Fe XANES and EXAFS were used to study the stability and the changes in the local atomic and the electronic structure upon repeated cycling (charging and discharging). Comparison of XANES peak positions of the powdered sample and the uncycled and cycled electrodes provides evidence that iron is predominantly in the Fe²⁺ state. The XANES reveals that Fe in LiFePO₄ even after repeated cycling is octahedrally coordinated by the oxygen. The EXAFS study reveals that there has been no change in the local atomic structure in the cycled LiFePO₄ electrodes, hence the material possesses very desirable characteristics for an electrode, which allows us to make LiFePO₄ an excellent choice for Li-ion battery applications. It will now be of further interest to make an in-situ investigation at different stages in the charging and discharging process and in different cycling stages to follow the structural and the electronic changes during the charge/discharge process.

References and Notes

(1) Ritchie, A. G. *J. Power Sources* **2001**, *96*, 1.

(2) Nishijima, M.; Takeda, Y.; Imanishi, N.; Yamamoto, O.; Takano, M. *J. Solid State Chem.* **1994**, *113*, 205.

(3) de Piecioto, L. A.; Thackeray, M. M. *Mater. Res. Bull.* **1986**, *21*, 583.

(4) Domingues, P. H.; Nunez, E.; Neto, J. M. *J. Magn. Magn. Mater.* **1991**, *96*, 101.

(5) Pernet, M.; Strobel, P.; Bonnet, B.; Bordet, P.; Chabre, Y. *Solid State Ionics* **1993**, *66*, 259.

(6) Fatseas, G. A.; Evain, M.; Ouvrard, G.; Brec, R.; Whangbo, M. H. *Phys. Rev. B* **1987**, *35*, 3082.

(7) Padhi, A. K.; Nanjundaswamy, K. S.; Masquelier, C.; Goodenough, J. B. *J. Electrochem. Soc.* **1997**, *144*, 2581.

(8) Masquelier, C.; Padhi, A. K.; Nanjundaswamy, K. S.; Goodenough, J. B. *J. Solid State Chem.* **1998**, *135*, 228.

(9) Padhi, A. K.; Nanjundaswamy, K. S.; Masquelier, C.; Okada, S.; Goodenough, J. B. *Electrochem. Soc.* **1997**, *144*, 1609.

(10) Nanjundaswamy, K. S.; Padhi, A. K.; Goodenough, J. B.; Okada, S.; Ohtsuka, H.; Arai, H.; Yamaki, J. *Solid State Ionics* **1992**, *92*, 1.

(11) Padhi, A. K.; Nanjundaswamy, K. S.; Goodenough, J. B. *J. Electrochem. Soc.* **1997**, *144*, 1188.

(12) Andersson, S.; Thomas, J. O.; Kalska, B.; Haggstrom, L. *Electrochem. Solid State Lett.* **2000**, *3*, 66.

(13) Amine, K.; Yasuda, H.; Yamachi, M. *Electrochem. Solid State Lett.* **2000**, *3*, 178.

(14) Yamada, A.; Chung, S. C. *J. Electrochem. Soc.* **2001**, *148*, A960.

(15) Yamada, A. Chung, S. C.; Hinokuma, K. *J. Electrochem. Soc.* **2001**, *148*, A224.

(16) Streltsov, V. A.; Belokoneva, E. L.; Tsirelson, V. G.; Hansen, N. K. *Acta Crystallogr. B* **1993**, *49*, 147.

(17) Bianconi, A. In *X-ray Absorption: Principles, Applications, Techniques of EXAFS, SEXAFS, and XANES*; Konongsberger, D. C., Prins, R., Eds.; John Wiley & Sons: New York, 1988; p 573.

(18) Manceau, A.; Gorshkov, A. I.; Drits, V. A. *Am. Mineral.* **1992**, *77*, 1133.

(19) Greines, L. A. *Phys. Rev. B* **1983**, *27*, 2111.

(20) Belli, M.; Scafati, A.; Bianconi, A.; Mobilio, S.; Palladino, L.; Reale, A.; Buratini, E. *Solid State Commun.* **1980**, *35*, 355.

(21) Glen, G. L.; Dodd, C. G. *J. Appl. Phys.* **1968**, *39*, 5372.

(22) Doeff, M. M.; Hu, Y.; McLarnon, F.; Kostecki, R. *Electrochem. Solid State Lett.* **2003**, *6*, A207.

(23) Ankudinov, A. L.; Ravel, B.; Rehr, J. J.; Conradson, S. D. *Phys. Rev. B* **1998**, *54*, 7565.

(24) Wilke, M.; Farges, F.; Petit, P. E.; Brown, G. E.; Martin, F. *Am. Mineral.* **2001**, *86*, 714.

(25) Calas, G.; Petiau, J. *Solid State Commun.* **1983**, *48*, 625.

(26) Berlier, G.; Spoto, G.; Fisicaro, P.; Bordiga, S.; Zecchina, A.; Giamello, E.; Lamberti, C. *Microchem. J.* **2002**, *71*, 101.

(27) Ng, H. N.; Calvo, C. *Can. J. Chem.* **1975**, *53*, 2064.

(28) Horne, C. R.; Bergmann, U.; Grush, M. M.; Perera, R. C. C.; Ederer, D. L.; Callcott, T. A.; Cairns, E. J.; Cramer, S. P. *J. Phys. Chem. B* **2000**, *104*, 9587.

(29) Garcia, J.; Benfatto, M.; Natoli, C. R.; Bianconi, A.; Fontaine, A.; Tolentino, H. *Chem. Phys.* **1989**, *132*, 295.

(30) Garcia, J.; Bianconi, A.; Benfatto, M.; Natoli, C. R. *J. Phys.* **1986**, *47*, C8.

(31) Davenport, A. J.; Bardwell, J. A.; Vitus, C. M. *J. Electrochem. Soc.* **1995**, *142*, 721.

(32) Schmuki, P.; Virtanen, S.; Davenport, A. J.; Vitus, C. M. *J. Electrochem. Soc.* **1996**, *143*, 721.

(33) Zabinsky, S. I.; Rehr, J. J.; Ankudinov, A.; Albers, R. C.; Eller, M. J. *Phys. Rev. B* **1995**, *52*, 2995.

(34) Ravel, B. *J. Synchrotron Radiat.* **2001**, *8*, 314.

(35) Kraus, W.; Nolze, G. Published by Bundesanstalt fuer Materialforchung und-pruefung, 1996.

(36) Thompson, H. A., Jr.; Brown, G. E.; Parks, G. A. *Am. Mineral.* **1997**, *82*, 48.